Jurnal Otomasi Kontrol dan Instrumentasi Vol 18 (2), 2026 ISSN: 2085-2517
https://doi.org/10.5614/joki.2026.18.2.1 E-ISSN: 2460-6340

Proportional-Controlled Microclimate Incubation System with IoT Monitoring for Dendrobium Seedling Acclimatization

Sistem Inkubasi Mikroklimat dengan Kendali Proporsional dan Pemantauan IoT untuk Aklimatisasi Bibit Dendrobium

[1]Al Barra Harahap *), [1]Vera Khoirunisa, [1]Nauval Abi Sopian, [1]Ahmad Rasya Mahfud

[1]Engineering Physics, Faculty of Industrial Technology, Institut Teknologi Sumatera, 35365, Lampung, Indonesia

*) *corresponding email: albarra.harahap@tf.itera.ac.id*

Abstract

Dendrobium orchid seedlings transferred from in vitro culture require stable microclimate conditions during acclimatization, particularly temperature, humidity, and photoperiod regulation, to improve adaptation to non-aseptic environments. However, quantitative evaluations of laboratory-scale incubation systems under constrained actuation conditions remain limited. This study presents a compact microclimate incubation system implementing proportional-only temperature control using fan-based unidirectional cooling, scheduled irrigation and lighting, and real-time IoT monitoring through a Node-RED dashboard. The system was developed using an ESP32-S3 controller and DHT22 sensors in a semi-enclosed multi-tier rack with a capacity of 360 seedling pots. Sensor calibration showed strong agreement with a reference instrument, achieving $R^2 > 0.99$ for temperature and humidity measurements. Temperature regulation at a reference value of 29.3 °C achieved a steady-state mean absolute error of 0.1 °C within a deviation range of −0.5 to +0.1 °C during 572 minutes of continuous operation, while maintaining all measurements within ±2 °C of the thermal tolerance range for Dendrobium acclimatization. Increasing proportional gain from K_p = 1000 to 2550 reduced the reference entry time from 362 s to 208 s. These findings demonstrate that proportional-only control with constrained cooling actuation can provide stable temperature regulation for compact indoor incubation systems.

Keywords: Proportional control; microclimate system; dendrobium acclimatization; unidirectional cooling; IoT monitoring

Abstrak

Bibit anggrek Dendrobium yang dipindahkan dari kultur in vitro memerlukan kondisi mikroklimat yang stabil selama tahap aklimatisasi, terutama pengaturan suhu, kelembaban, dan fotoperiode, untuk mendukung adaptasi terhadap lingkungan non-aseptik. Namun, evaluasi kuantitatif terhadap sistem inkubasi skala laboratorium dengan keterbatasan aktuasi masih terbatas. Penelitian ini menyajikan sistem inkubasi mikroklimat kompak yang menerapkan kendali suhu proporsional dengan mekanisme pendinginan satu arah berbasis kipas, penyiraman dan pencahayaan terjadwal, serta pemantauan IoT waktu nyata melalui dasbor Node-RED. Sistem dikembangkan menggunakan mikrokontroler ESP32-S3 dan sensor DHT22 pada struktur rak bertingkat semi-tertutup dengan kapasitas hingga 360 pot bibit. Hasil kalibrasi sensor menunjukkan kesesuaian yang kuat terhadap instrumen referensi dengan nilai $R^2 > 0,99$ untuk pengukuran suhu dan kelembaban. Kendali suhu pada nilai referensi 29,3 °C menghasilkan mean absolute error kondisi tunak sebesar 0,1 °C dalam rentang deviasi −0,5 hingga +0,1 °C selama 572 menit operasi kontinu, dengan seluruh pengukuran berada dalam batas toleransi termal ±2 °C untuk aklimatisasi Dendrobium. Peningkatan penguatan proporsional dari K_p = 1000 menjadi 2550 menurunkan waktu mencapai suhu referensi dari 362 detik menjadi 208 detik. Hasil ini menunjukkan bahwa kendali proporsional dengan keterbatasan aktuasi pendinginan mampu menghasilkan regulasi suhu yang stabil pada sistem inkubasi dalam ruangan berukuran kompak.

Kata Kunci: Kontrol proporsional; sistem mikroklimat; aklimatisasi dendrobium; pendinginan satu arah; pemantauan IoT

Paper accepted April 17th, 2026 – paper revised June 16th, 2026– approved June 29th, 2026

This paper is open access with CC BY-SA *license*.

1 Introduction

Controlled environment systems are increasingly utilized in small-scale cultivation, experimental, and laboratory settings to reduce environmental variability and improve process repeatability [1], [2]. In such systems, key environmental variables, including air temperature and relative humidity, must be continuously monitored and regulated relative to operating conditions, while lighting is typically implemented as a controlled photoperiod and

treated as a time-defined energy input [3]. These requirements introduce challenges related to sensor reliability, actuator coordination, and real-time control implementation, particularly in systems with limited actuation capability.

One application with particularly stringent microclimate requirements is the acclimatization of Dendrobium orchid seedlings produced through in vitro tissue culture. During this transition phase, seedlings must adapt from aseptic culture conditions to non-aseptic environments while remaining sensitive to variations in temperature, humidity, and light. Published acclimatization protocols report optimal conditions at 25 ± 2 °C with relative humidity of 70–85%, a 12-hour photoperiod, and light intensities ranging from 13 to 60 $\mu mol \cdot m^{-2} \cdot s^{-1}$ PPFD depending on species and acclimatization stage [4], [5], requirements that demand consistent and repeatable environmental delivery. In tropical regions such as Lampung, Indonesia, indoor ambient conditions exhibit considerable diurnal variability, making manual regulation insufficient for maintaining the stability required during this critical growth phase.

Previous studies have reported automated incubation and greenhouse systems integrating microcontrollers, environmental sensors, and actuators for support [6], [7]. Akkaş and Sokullu [6], for instance, showed that sensor node placement and communication protocol selection critically affect data reliability in wireless IoT greenhouse monitoring, an observation that underscores the importance of sensor characterisation in deployment-grade systems. These systems commonly employ temperature and humidity sensing, time-based scheduling via real-time clocks, and control strategies ranging from on-off switching and proportional control to PID and rule-based approaches [8], [9]. IoT-based monitoring platforms have also been integrated into such systems to enable remote data visualization and real-time actuator supervision, including Node-RED-based dashboard implementations for multi-parameter environmental monitoring [10], [11]. Cicioğlu and Çalhan [12] further demonstrated that multi-tier IoT architectures support remote parameter adjustment and real-time monitoring across distributed agricultural environments, a functionality that motivates the monitoring subsystem design adopted in this work. While these works collectively demonstrate the feasibility of automated environmental regulation, their reported performance is closely tied to system integration quality, sensor characteristics, and control response behavior. Specifically, systematic reporting of sensor calibration linearity, gain-dependent control response characterisation, and quantified steady-state deviation bounds under continuous operation remains limited, particularly in studies focused on laboratory-scale incubation platforms with constrained actuation [7], [8].

This reporting gap is consequential for application-driven systems: the ability to verify that steady-state temperature deviation remains within the biological tolerance of the target organism, in this case $\pm 2\ ^{\circ}C$ for Dendrobium acclimatization [4], is a prerequisite for assessing operational suitability. Systematic characterisation of sensor behavior, control response across gain settings, and long-duration steady-state performance under practical indoor conditions is therefore necessary to establish documented and comparable performance data for laboratory-scale incubation platforms.

Based on this gap, this study presents a proportional-controlled microclimate incubation system with IoT-based monitoring for Dendrobium seedling acclimatization. The system integrates an ESP32-S3 microcontroller, DHT22 sensors, real-time clock–based scheduling, and multiple actuators for temperature regulation through fan-based cooling, scheduled irrigation, and photoperiod control. A Node-RED–based IoT monitoring dashboard deployed on an edge computing platform provides real-time visualization and remote parameter adjustment. The system is evaluated from an engineering performance perspective, using Dendrobium seedlings as application context. The contributions of this work are threefold: (1) the design and implementation of a microclimate incubation system for indoor laboratory-scale acclimatization; (2) the application and characterisation of proportional-only control for indirect temperature regulation under a passive unidirectional cooling constraint; and (3) the integration and evaluation of an IoT-based monitoring platform for real-time environmental supervision and quantitative steady-state performance assessment.

2 Method

2.1 System Architecture

The proposed incubation system consists of four main subsystems: sensing, control, actuation, and monitoring, implemented within a semi-enclosed chamber that allows passive air exchange with the surrounding indoor environment. The overall architecture and the interaction between these subsystems are illustrated in Fig. 1. Environmental sensing is carried out using DHT22 sensor to measure air temperature and relative humidity. A real-time clock (RTC) provides time references for scheduled operations. All sensing, control, and scheduling processes are executed by an ESP32-S3 microcontroller as the central control unit.

The actuation subsystem includes DC fans, a water pump, and LED plant lights. Temperature regulation is achieved through fan-based air circulation using proportional-only control with unidirectional cooling, reflecting the absence of active heating.

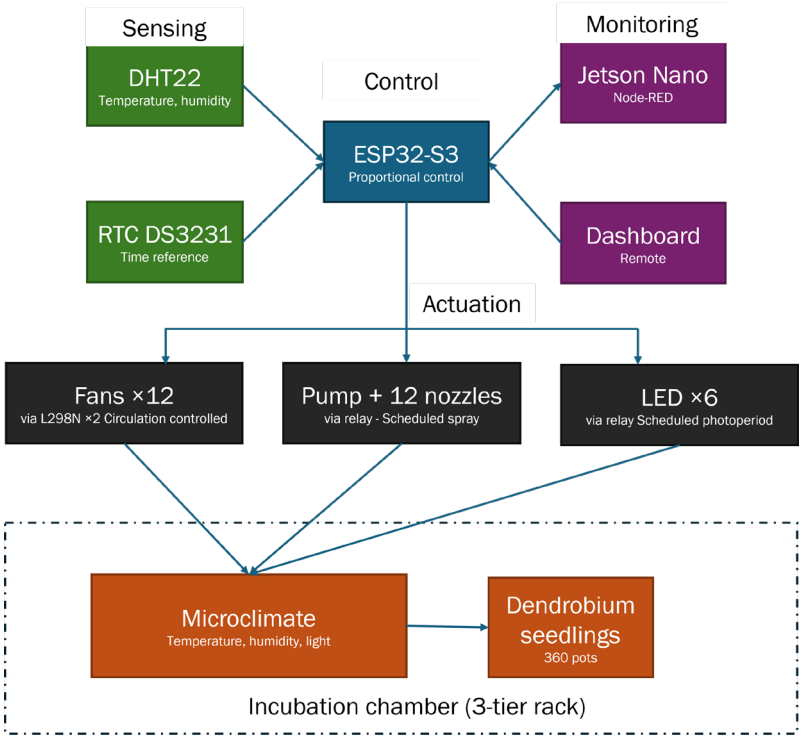


Figure 1. System architecture showing the interaction between the four subsystems: sensing, control, actuation, and monitoring

The monitoring subsystem provides real-time visualization of environmental variables and actuator states through a Node-RED dashboard deployed on an NVIDIA Jetson Nano, which serves as the edge computing platform for data aggregation and visualization, consistent with IoT-based monitoring approaches that integrate edge hardware with visual dashboard interfaces for real-time environmental supervision [11], [13]. Data exchange between the ESP32-S3 and the Jetson Nano is implemented over the MQTT protocol (port 1883) using an asynchronous client, enabling real-time transmission of sensor readings and remote adjustment of the temperature reference and proportional gain.

2.2 Hardware Configuration

The incubation system is implemented using a multi-tier rack structure (length 111.5 cm × width 33.5 cm × height 60 cm) within a semi-enclosed chamber for laboratory-scale operation. The rack consists of three tiers, each accommodating up to 120 Dendrobium seedling pots, for a total capacity of 360 pots.

The key hardware components, quantities, microcontroller pin assignments, and calibration references are summarized in Table 1. Sensors and actuators are physically distributed across the rack to represent the overall chamber condition and ensure coverage of the cultivation area. The ESP32-S3 microcontroller interfaces with the sensing units, a real-time clock (RTC) module, and actuator driving circuits.

Air circulation is provided by multiple 12 V DC axial fans distributed across the rack structure and driven using L298N motor driver modules. The fans operate as two-wire DC units without speed feedback. Water distribution is implemented using spray nozzles connected to a DC pump, while LED plant lights are controlled through relay modules. Both spraying and lighting are operated based on predefined schedules. The spatial distribution of water delivery was characterized by measuring the water volume collected at each pot position during a 2-minute spraying operation, with four nozzles arranged horizontally at a height of 40 cm above each tier. The resulting distribution map was constructed by interpolating the measured values across the cultivation grid. Similarly, the spatial distribution of LED lighting intensity was characterized by measuring illuminance using a lux meter at a distance of 30 cm from the LED unit at each pot position, with the LED mounted vertically at the corner of each tier inclined at 60 degrees toward the plant area. Both distribution maps were obtained under controlled conditions using a single representative unit and subsequently used to characterize the spatial uniformity of environmental inputs across the cultivation area, as presented in the Results section.

Table 1. Key hardware components and instrumentation used in the incubation system, including quantity, microcontroller pin assignment, and calibration reference where applicable

Component	Qty	Pin (ESP32-S3)	Calibration Reference
YD-ESP32-S3 WROOM 16MB Flash 8MB PSRAM	1	—	—
DS3231 - generic no brand	1	I2C (SDA : GPIO 8 /SCL : GPIO 9)	—
NVIDIA Jetson Nano - NVIDIA USA	1	Wi-Fi / MQTT	—
DHT22 - generic no brand	1	GPIO 40	UNI-T UT333
DC axial fan 12V 120x120mm - generic no brand	6	ENA1 GPIO32 IN1 GPIO33 IN2 GPIO25 IN3 GPIO26 IN4 GPIO27 ENB2 GPIO14	—
DC axial fan 12V 120x120mm - generic no brand	6	ENA3 GPIO19 IN1 GPIO18 IN2 GPIO5 IN3 GPIO17 IN4 GPIO16 ENB4 GPIO4	—
L298N dual H-bridge - generic no brand	2	See fan pins above	—
Sinleader 12V 80PSI sprayer pump	1	—	—
0.6mm mist nozzle - generic no brand	12	—	Taffware digital scale max. 3 kg (flow rate calibration mL per 2 min per pot position)
5V relay - generic no brand	2	GPIO38 (LED lights) GPIO37 (pump)	—
Taffware SMD 2835 50W 220V red-blue grow light	6	—	UNI-T UT383

As illustrated in Fig. 2, a single DHT22 sensor is installed within the rack to measure the internal air temperature, while each tier is equipped with two inlet fans (one side and one rear) and two outlet fans (one side and one rear) for air circulation, four spray nozzles for irrigation, and two LED units for photoperiod lighting, giving a total of one DHT22 sensor, twelve fans, twelve nozzles, and six LED units across the three-tier rack.

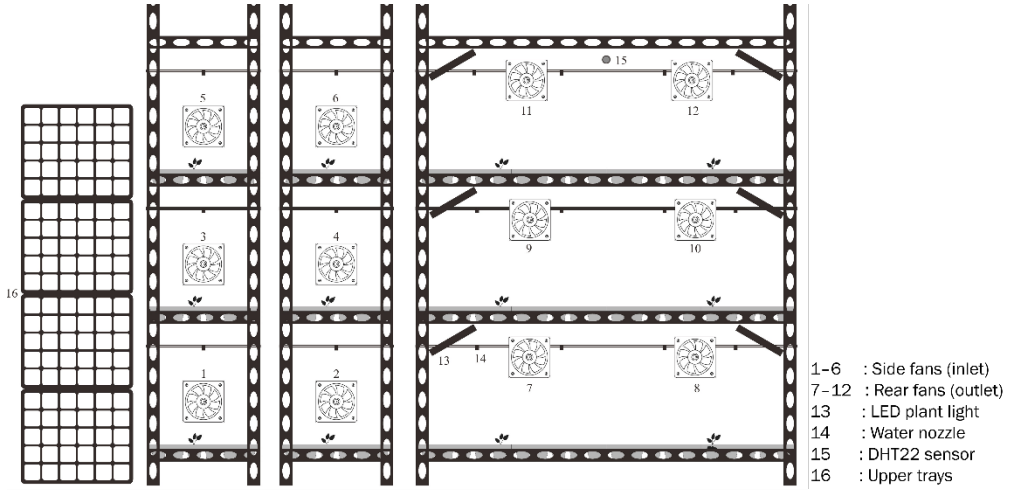


Figure 2. Physical layout of the multi-tier incubation rack system within the semi-enclosed chamber

2.3 Software and Control Strategy

The embedded software is implemented on the ESP32-S3 platform to perform sensor data acquisition, control computation, actuator switching, and data transmission to the monitoring interface. Temperature and relative humidity are sampled once per control cycle at approximately 100 ms intervals using the DHT22 sensor, consistent with the delay(100) execution period at the end of each control loop iteration. The measured temperature is processed using a linear calibration model. A user-defined temperature reference T_{ref} and proportional gain K_p are provided through the monitoring interface and can be adjusted during operation.

Temperature regulation is implemented using proportional control with fan-based cooling. The control error is defined as

$$e(t) = \mathrm{T(t)} - T_{ref} \quad (1)$$

where $T(t)$ denotes the measured air temperature at time t. Cooling is activated only when $e(t) > 0$. The control input is given by

$$u(t) = \mathrm{sat}_{[0,255]}\left(K_p\, e(t)\right) \quad (2)$$

where $sat_{[0,255]}$ denotes a saturation function limiting the proportional control output $K_p e(t)$ within the actuator range of 0–255. The control signal $u(t)$ is mapped to a pulse-width modulation (PWM) duty cycle that drives the DC fan. PWM output is generated using the Arduino-ESP32 analogWrite() function at a default frequency of approximately 1 kHz with 8-bit resolution (0–255).

The temperature regulation logic is illustrated in Fig. 3. Water spraying and LED lighting are operated using predefined schedules based on the real-time clock (RTC) and are not included in the closed-loop control.

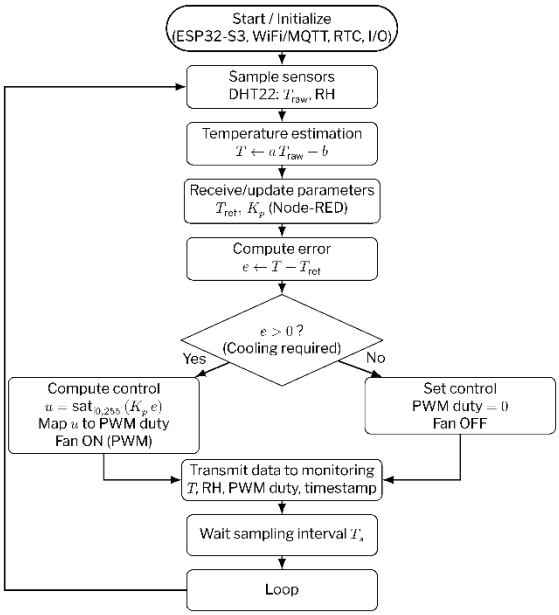


Figure 3. Flowchart of the proportional-based unidirectional temperature regulation implemented on the ESP32-S3

2.4 Experimental Procedure and Performance Evaluation

Experimental evaluation was conducted under air-conditioned indoor laboratory conditions, with the room temperature maintained at approximately 27 °C and relative humidity of approximately 90% throughout the testing period, as measured using a handheld reference instrument prior to each test session. The evaluation focuses on sensor performance, temperature regulation behavior, scheduled subsystem operation, and monitoring functionality.

Sensor performance was evaluated through calibration by comparing DHT22 measurements of air temperature and relative humidity against a reference instrument. The evaluation considers measurement deviation, linearity, and repeatability within the operating range.

Temperature regulation performance was evaluated by observing the temporal response under proportional control. Transient response experiments were conducted using three proportional gain values (K_p = 1000, 1500, and 2550), each evaluated in a single continuous observation window of approximately 550 seconds following system activation. Long-duration steady-state performance was subsequently evaluated at K_p = 2550 over a single continuous session of approximately 660 minutes (06:00–18:00), of which 572 minutes constituted the steady-state evaluation window following LED activation and system stabilization. Each test condition was evaluated once. Performance indicators include the time required to first reach the reference temperature (t_{enter}), the time required to enter and remain within a bounded operating region (t_{band}), defined as the interval $[Tref - 0.5, Tref + 0.1]$ °C within which the system is considered to be in steady-state operation, and the

resulting steady-state temperature range relative to the reference. All reported temperature values are rounded to one decimal place, consistent with the $0.1\ °C$ resolution of the DHT22 sensor.

2.5 Seedling Preparation

Prior to placement in the incubation system, the seedlings were prepared through a standardized handling procedure. The plantlets were removed from in vitro culture, cleaned to remove residual media, rinsed with clean water, and subjected to a brief soaking process using a fungicide solution followed by a vitamin B1 solution. The seedlings were then air-dried and placed in soft pots containing moss-based growing media [14]. A small amount of slow-release fertilizer (approximately three granules) was applied on top of each growing medium at the initial setup stage, and no additional fertilization was provided during the observation period. This procedure was applied consistently to all samples to ensure uniform initial handling conditions. The plant material consisted of six Dendrobium types: *D. Champagne*, *D. Arhadea*, *D. Budiono Lamtoro*, *D. Phyllis*, *D. Kaifano*, and *D. Sutikno*. The six types were distributed unevenly across the three rack tiers, reflecting the availability of seedlings at the time of placement rather than a controlled experimental design.

3 Results and Discussion

3.1 Sensor Performance

The performance of the DHT22 sensors was evaluated through calibration against a reference instrument for air temperature and relative humidity, as showed in Fig. 4. To assess the measurement consistency of low-cost unbranded DHT22 sensors, two units (designated A and B) were calibrated against the reference instrument under identical conditions. One unit was subsequently installed in the incubation system for temperature control, while the calibration of both units is reported here to demonstrate the repeatability of this sensor type.

For temperature measurement, both sensors showed a strong linear relationship with the reference instrument. The calibration equations and R^2 values for all four sensor-parameter combinations are annotated directly in Fig. 4, with R^2 values of 0.997 for both temperature sensors and $0.991 - 0.992$ for relative humidity sensors. The fitted equations are $T = 1.0435 \cdot T_{raw} - 1.3256$ for DHT22 A and $T = 1.0352 \cdot T_{raw} - 1.0993$ for DHT22 B, with humidity equations of $RH = 0.9530 \cdot RH_{raw} + 1.7460$ and $RH = 0.9672 \cdot RH_{raw} + 0.4022$ respectively. These results confirm consistent and repeatable sensor response across the operating range. The observed calibration agreement is adequate for proportional control, where systematic offset is of greater concern than random variation. Although relative humidity is not included in the control loop, the measurements are used for environmental monitoring during system operation.

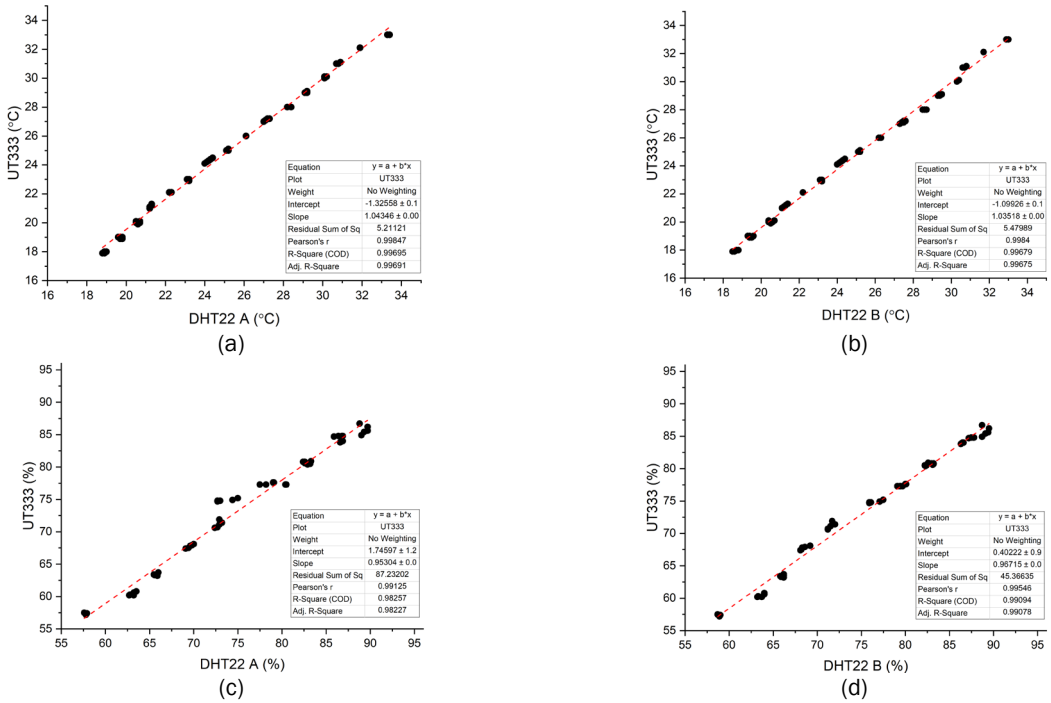


Figure 4. Calibration results of (a, b) DHT22 temperature and (c,d) relative humidity sensors against a reference instrument

Both temperature and relative humidity calibrations were performed against a UNI-T UT333 reference instrument. Prior to calibration, the raw sensor readings showed a mean absolute error of $0.51\ °C$ and $0.20\ °C$ for DHT22 A and DHT22 B respectively for temperature, and 4.60% and 2.02% for relative humidity, with corresponding RMSE values of $0.57°\ C$, $0.22\ °C$, 5.23%, and 2.82% (n = 50). These deviations are consistent with the manufacturer-specified accuracy of $\pm 0.5\ °C$ and ±2–5% RH for the DHT22 sensor, and are corrected through the linear calibration equations applied in the embedded firmware.

3.2 Temperature Control

The temperature response under proportional control shows a consistent monotonic decrease toward the reference without overshoot for all tested gain values. A step-like pattern is also observed, reflecting the discrete nature of the control action and sensor resolution. These characteristics are illustrated in Fig. 5, where the initial temperature is approximately $30\ °C$ following LED activation.

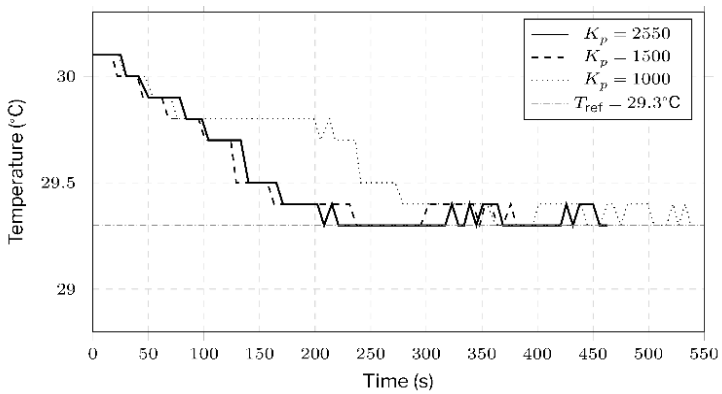


Figure 5. Temperature responses under proportional-only unidirectional cooling for three proportional gain values (K_p = 1000, 1500, 2550 with $T_ref = 29.3$ °C)

Performance is evaluated using three indicators: the time required to first reach the reference t_{enter}, the time required to enter and remain within a bounded range t_{band}, and the resulting temperature range during operation, as summarized in Table 2. The results show that increasing K_p reduces the time required to reach the reference. For example, $K_p = 1000$ requires 362 s, while $K_p = 2550$ reduces this time to 208 s. A similar trend is observed in t_{band} when increasing K_p from 1000 to 1500, indicating faster convergence into the operating region. However, further increase in K_p does not consistently improve t_{band}, indicating that the response is influenced by factors beyond the controller gain. In contrast, the temperature range remains similar across all gain values $(29.3 - 30.1\ °C)$, indicating that steady-state behavior is less sensitive to gain variation. Overall, these data confirm that lower gain values lead to slower response, while higher gain values improve transient performance but provide limited additional benefit in steady-state behavior.

Table 2. Response indicators for proportional gain selection under unidirectional cooling.

K_p	$t_{\text{enter}}(s)$	$t_{\text{band}}(s)$	Temperature range (°C)
1000	362	279	29.3–30.1
1500	237	163	29.3–30.1
2550	208	171	29.3–30.1

The presence of actuator saturation also explains why increasing K_p beyond a certain range does not significantly improve performance. As $K_p e(t)$ (eq. 2) approaches the saturation limit, the actuator operates near its maximum capacity, and further increase in gain does not produce a proportional increase in control effect. This behavior is reflected in Table 2, where increasing K_p from 1500 to 2550 does not significantly reduce t_{band}.

This behavior follows directly from the structure of the proportional control law in Eq. (2): once the product Kp·e(t) reaches the PWM ceiling of 255, increasing gain no longer produces additional cooling effect, regardless of the error magnitude. Similar gain-limited performance under constrained actuation has been noted in comparable low-cost temperature regulation systems [7], [8].

The saturation threshold for each gain value can be derived directly from the control law in Eq. (2): saturation occurs when $Kp \cdot e(t) \geq 255$, corresponding to error thresholds of 0.26 °C, 0.17 °C, and 0.10 °C for K_p = 1000, 1500, and 2550, respectively. At K_p = 2550, the actuator reaches full output at an error of only 0.1 °C above the

reference, meaning the fan operates at maximum capacity for most of the transient phase whenever temperature exceeds 29.4 ℃. This deep saturation condition explains why tband at K_p = 2550 (171 s) shows no improvement over K_p = 1500 (163 s): once full cooling capacity is engaged, further gain increase yields no additional effect. The practical gain range for this system is therefore bounded between Kp = 1000 and Kp = 1500, where the proportional zone remains sufficiently wide to produce a meaningful variation in cooling intensity.

The system behavior under long-duration operation is shown in Fig. 6, where the pre-LED ambient temperature of approximately 27.3 ℃ is visible in the initial portion of the record. Upon LED activation, internal heat generation drives the temperature upward, which is subsequently regulated by the control system. During steady operation, the temperature remains within a bounded range around the reference, as also reflected in Table 3, where the system achieved a mean absolute error of $0.1\ °C$ and operates within a deviation band of -0.5 to $+0.1\ °C$. It should be noted that the reported MAE of $0.1\ °C$ coincides with the $0.1\ °C$ measurement resolution of the DHT22 sensor; the steady-state error is therefore at or near the measurement floor, and finer error quantification would require a higher-resolution reference sensor.

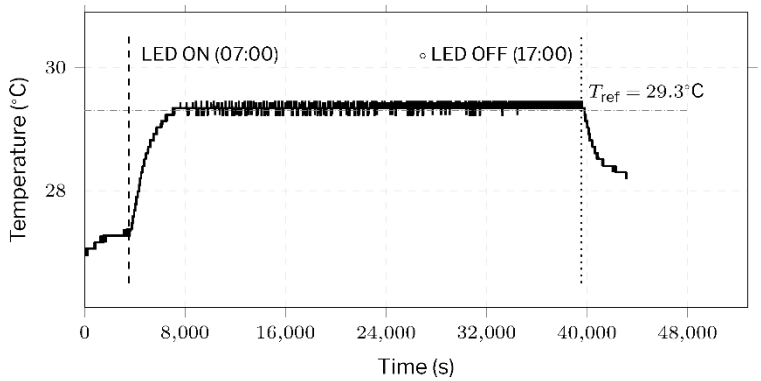


Figure 6. Long-duration temperature response under proportional-based unidirectional cooling ($K_p = 2550$)

The long-duration record also permits characterisation of the system's response to the LED-induced thermal disturbance. Upon LED activation, the internal temperature rose toward the reference, reaching a peak of 29.4 ℃, a disturbance magnitude of approximately +2.2 ℃ relative to the pre-activation ambient level. The system entered stable operation within $T_{ref} \pm 0.5$ ℃ approximately 28 minutes after LED activation, with the temperature remaining at or below $29.4\ °C$ throughout the 660-minute observation period (including 572 minutes of steady-state evaluation). The absence of upper band violations indicates that the proportional controller, despite its structural limitation to cooling-only actuation, was effective in bounding the thermal response within the target operating range throughout continuous LED illumination.

Relative humidity during the 572-minute steady-state window ranged from 74.2% to 83.9%, with a mean of 79.1%, recorded passively without closed-loop regulation. This range falls within the 70–85% relative humidity recommended for Dendrobium acclimatization [4].

Table 3. Quantitative steady-state temperature regulation performance evaluated over the stabilized operating window under continuous LED illumination

Parameter	Value
Reference temperature, T_{ref} (℃)	29.3
Steady-state mean temperature, $\bar{T}_{ss}$ (℃)	29.3
Mean absolute error (MAE) (℃)	0.1
Steady-state RMSE (℃)	0.1
Steady-state deviation band (℃)	$+0.1 / -0.5$
Evaluation window duration (min)	572
Pre-LED ambient temperature (℃)	27.3
LED-on disturbance magnitude (℃)	+2.2
Time to stable operation after LED on (min)	28
Peak temperature during transient (℃)	29.4
Upper deviation band violations	0
Sample within ±2℃ of T_{ref} (%)	100.0

Based on these observations, the control system operates by limiting the temperature rise caused by internal heat sources rather than reducing the temperature below ambient conditions. The achievable performance is therefore constrained by the ambient temperature and the available cooling mechanism. Despite these limitations, the system is able to maintain stable temperature behavior under continuous disturbance, with bounded fluctuations around the reference.

3.3 Environmental Response to Scheduled Spraying and Lighting

Water spraying and LED plant lighting are operated using predefined schedules and act as time-based inputs during system operation. The lighting system is activated daily from 07:00 to 17:00, while the spraying system is operated once per day at 06:20 for 2 minutes. These scheduled operations define repeatable environmental inputs during system operation.

Fig. 7 illustrates the spray distribution across the cultivation rack. Fig. 7(a) shows the spray coverage of a single nozzle, which is used as the base characteristic and is obtained using a 12 V pump with a rated pressure of 80 psi and a flow rate of 3.1 LPM under a single-nozzle condition. This distribution is then interpolated and superimposed for four nozzles arranged in series along the rack with a spacing of approximately 27 cm, resulting in the overall spray pattern shown in Fig. 7(b). A grid is used to represent the positions of individual plant containers. The distribution indicates higher water volume near the nozzle centers and lower values toward the outer regions, with a range from approximately 0.4 mL to 4.6 mL based on the scale shown in Fig. 7(c). Overlapping regions between adjacent nozzles are observed, leading to non-uniform water distribution across the cultivation area. In the actual system, the pump supplies four nozzles per rack across three rack levels. The combined distribution is derived from the characteristic of a single nozzle, while variations between nozzles may occur due to manufacturing differences or operating conditions and are not explicitly modeled.

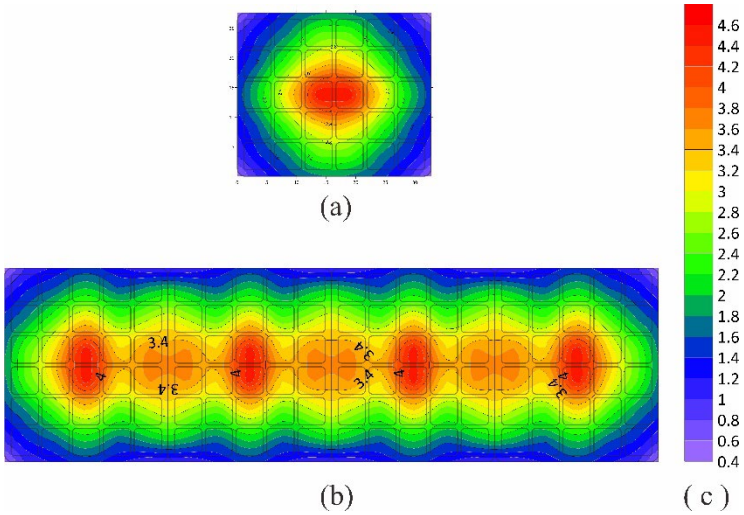


Figure 7. Water spraying distribution during a 2-minute scheduled operation: (a) spray coverage of a single nozzle, (b) combined coverage across one rack of four trays arranged horizontally, and (c) delivered water volume scale in milliliters. Each tray measures 32.7 cm (length) × 27.6 cm (width) × 4.6 cm (height); the horizontal axis in (b) therefore spans 130.8 cm across the four trays, and the vertical axis spans 27.6 cm.

Fig. 8 shows the spatial distribution of LED lighting intensity across the cultivation rack. The lighting system consists of two LED units positioned on the left and right sides, mounted vertically and inclined at approximately 60 degrees toward the plant area. A grid is used to represent the positions of individual plant containers (soft pots with moss-based growing media). The light intensity ranges from approximately 400 lux at the outer regions to about 3000 lux near the light sources, with an average value around 1200 lux. The measurements are obtained using a luxmeter at a distance of 30 cm from the lowest part of the LED unit and interpolated based on the measured characteristics of a single LED under controlled dark-room conditions. The distribution indicates that light intensity varies across the cultivation area depending on the distance from the light sources.

The LED units used were narrow-band red-blue grow lights (SMD 2835, 50 W), which emit primarily at wavelengths of approximately 450 nm (blue) and 660 nm (red). Light intensity was recorded in lux using a lux meter; however, lux meters are calibrated to the photopic response of the human eye and substantially underestimate illuminance from narrow-band red-blue sources, as these wavelengths fall outside the peak of the photometric sensitivity function. Consequently, the recorded lux values cannot be reliably converted to PPFD without the spectral power distribution data of the specific LED unit, which was not available in this study. The reported lux values should therefore be understood as relative spatial distribution indicators rather than absolute measures of photosynthetically active radiation.

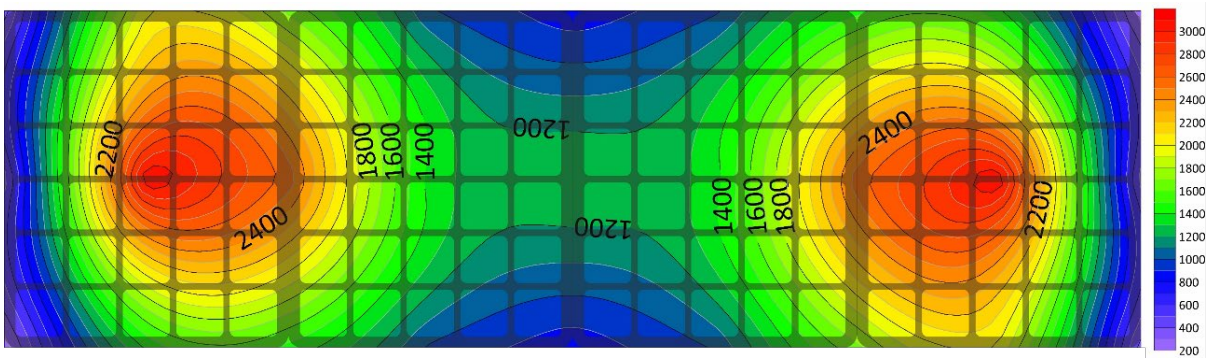


Figure 8 Spatial distribution of LED plant lighting intensity (lux) across a single cultivation rack of four trays arranged horizontally. Each tray measures 32.7 cm (length) × 27.6 cm (width); the horizontal axis therefore spans 130.8 cm across the four trays, and the vertical axis spans 27.6 cm.

3.4 System Monitoring and Data Logging Performance

The monitoring system is implemented using a Node-RED–based web interface for real-time visualization of temperature, relative humidity and actuator states, as shown in Fig. 9. Data is recorded continuously during system operation. Monitoring performance is evaluated based on the data transmission delay between the embedded controller and the database over four consecutive days, each with approximately 12 hours of runtime. The results, summarized in Table 4, show that the transmission delay ranges from 2 to 17 s, with an average of approximately 3 s across all test days.

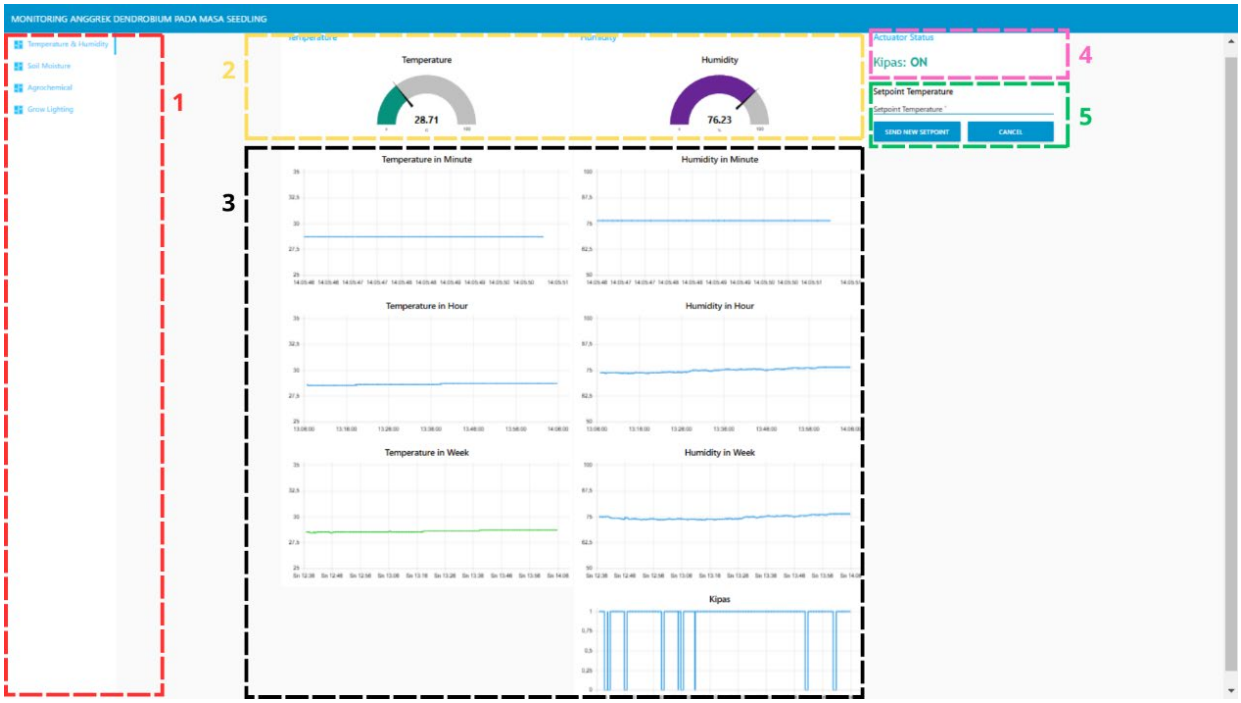


Figure 9 Node-RED–based monitoring dashboard deployed on NVIDIA Jetson Nano, consisting of: (1) navigation menu for subsystem selection, (2) real-time gauges for temperature and relative humidity, (3) time-series charts for temperature, humidity, and fan actuator state across minute, hour, and weekly intervals, (4) actuator status indicator, and (5) setpoint input panel for remote adjustment of the temperature reference and proportional gain.

The control loop is executed locally on the ESP32-S3 platform and operates independently of the monitoring system. As a result, variations in data transmission delay do not influence temperature regulation process, which is based on local sensor feedback.

Table 4. Summary of data transmission delay during IoT tests

Test day	Data count	Min (s)	Max (s)	Mean (s)
Day 1	8,885	2	16	3.22
Day 2	9,194	2	13	3.11
Day 3	9,501	2	17	3.12
Day 4	8,579	2	14	3.38

3.5 Operational Outcomes on Seedling Viability

Seedling viability is used as an operational indicator of environmental suitability during system operation. After 31 days of continuous operation, 354 of the 360 seedlings (98.3%) remained viable, as shown in Fig. 10, with 51 seedlings exhibiting shoot emergence. The number of surviving seedlings per tier was 118, 120, and 116 for the upper, middle, and lower tiers respectively, while shoot emergence was most frequent in the lower tier (30 seedlings) compared to the middle (12) and upper (9) tiers. Variations in survival and shoot emergence across rack tiers were observed; however, these differences are not directly attributed to specific environmental parameters or control performance, but instead reflect the combined influence of initial plant conditions and spatial variations in the cultivation environment.

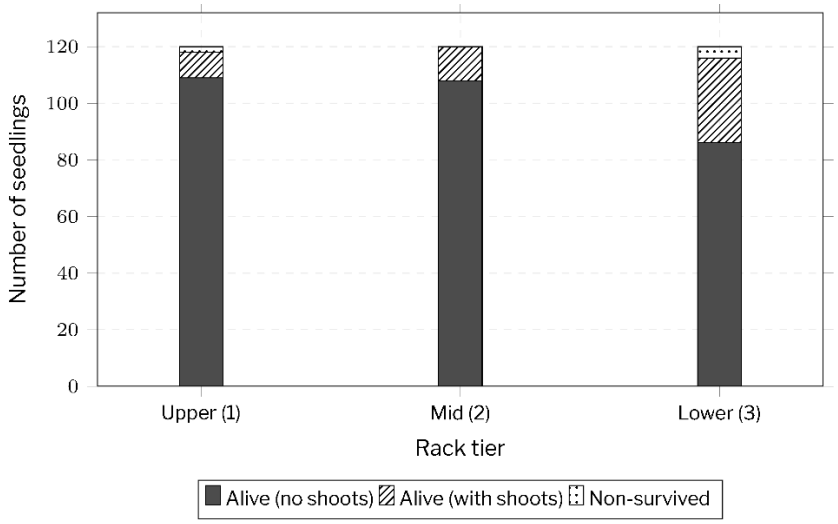


Figure 10 Aggregated distribution of seedling viability categories across rack tiers after 31 days of incubation system operation

3.6 Discussion

Proportional-only control with fan-based cooling maintained stable indoor temperature under sustained LED-generated heat input. The monotonic cooling response without overshoot across all tested gain values follows directly from the unidirectional actuation constraint: the control output is bounded above by actuator saturation and below by zero, making overshoot structurally impossible regardless of gain. Reference entry time decreased from 362 s at K_p = 1000 to 208 s at K_p = 2550, confirming that proportional gain modulates cooling intensity within the actuator operating range. The diminishing improvement in t_{band} beyond K_p = 1500 is explained by actuator saturation: at K_p = 2550, the control signal $Kp \cdot e(t)$ reaches the PWM ceiling at an error of 0.1 ℃, meaning full cooling capacity is engaged throughout most of the transient phase and further gain increase yields no additional effect. The practical gain range for this system therefore lies between K_p = 1000 and K_p = 1500, where transient improvement is most pronounced. This gain-limited behavior is consistent with established findings on actuator saturation in proportional-type control, where tracking performance improves with increasing gain only up to a threshold, beyond which saturation causes the benefit to diminish [15]. Güney and Çakır [9] reported steady-state convergence within 260 s using an optimized PID controller with bidirectional actuation; the present system achieved a comparable entry time under a more restrictive unidirectional constraint, with a steady-state MAE of 0.1 ℃, within the ±2 ℃ thermal tolerance specified for Dendrobium acclimatization [4].

The step-like pattern in the temperature response reflects the combined effect of DHT22 sensor resolution and discrete PWM actuation, consistent with calibration behavior reported for low-cost environmental sensors [16]. IoT transmission delays averaged 3 s with a maximum of 17 s across four test days, consistent with Node-RED-based agricultural monitoring architectures [13], these delays do not affect temperature regulation, which executes locally on the ESP32-S3 independent of the network path.

The spray distribution non-uniformity (0.4–4.6 mL per pot position) arises from overlapping nozzle coverage under a fixed single-pump configuration, while lighting intensity variation (400–3000 lux, average ~1200 lux) reflects the fixed geometry of the LED units. Together, these gradients produce position-dependent cultivation conditions across the rack. Seedling viability and shoot emergence after 31 days of operation indicate that the incubation environment remained within acceptable bounds throughout the evaluation period; tier-level differences in outcomes are attributed to the combination of environmental gradients and initial seedling variability rather than to control performance.

Several limitations of the present implementation are worth noting. The cooling mechanism is unidirectional: the system can only reduce temperature above the reference and cannot actively drive it below ambient. Evaluation was conducted at a single operating point ($T_{ref} = 29.3\ °C$), and robustness across multiple setpoints was not assessed. Each gain value was evaluated in a single test run, and repeatability across multiple runs was not assessed. No integral or derivative control action was employed, and humidity was monitored but not regulated in a closed loop. The spray and lighting distributions were characterized using a single representative unit; nozzle-to-nozzle and LED-to-LED variation was not measured. Future work should address these limitations by incorporating bidirectional thermal actuation, evaluating multi-setpoint robustness, introducing integral action to reduce residual offset, and directly measuring PAR using a calibrated quantum sensor to allow quantitative comparison with Dendrobium acclimatization protocols.

4 Conclusion

This study presented the design, implementation, and quantitative evaluation of a compact laboratory-scale incubation system for Dendrobium orchid seedling acclimatization. The work was motivated by the limited availability of systematic performance data for indoor incubation platforms operating under constrained actuation conditions, a gap that restricts the reproducibility and comparability of such systems in practical settings.

The implemented system demonstrated that proportional-only control combined with fan-based cooling is sufficient to maintain stable temperature behavior under continuous indoor operation. Sensor calibration yielded strong agreement with a reference instrument across both DHT22 units ($R^2 > 0.99$), confirming measurement consistency within the operating range. Temperature regulation achieved a mean absolute error of $0.1\ °C$ within an asymmetric steady-state deviation band of -0.5 to $+0.1\ °C$ over a continuous 572-minute evaluation window. These results provide documented performance data for compact incubation systems operating with passive cooling constraints and proportional-only control. From a practical standpoint, these findings suggest that proportional-only control with passive unidirectional cooling constitutes a structurally simpler control approach suitable for low-cost incubation systems where temperature regulation within a $\pm 2\ °C$ tolerance is the primary objective.

Acknowledgement

The authors would like to acknowledge the financial support provided by the Institut Teknologi Sumatera (ITERA) through the 2024 Internal Research Grant under the Penelitian Dosen Pemula scheme. This support enabled the design, implementation, and experimental evaluation of the incubation system reported in this study.

Reference

[1] N. Gruda, M. Bisbis, and J. Tanny, "Impacts of protected vegetable cultivation on climate change and adaptation strategies for cleaner production – A review," *Journal of Cleaner Production*, vol. 225, pp. 324–339, Jul. 2019, https://doi.org/10.1016/j.jclepro.2019.03.295.

[2] R. Shamshiri *et al.*, "Advances in greenhouse automation and controlled environment agriculture: A transition to plant factories and urban agriculture," *International Journal of Agricultural and Biological Engineering*, vol. 11, no. 1, pp. 1–22, Jan. 2018. [Online] Available : https://ijabe.org/index.php/ijabe/3210

[3] J. A. Nelson and B. Bugbee, "Economic Analysis of Greenhouse Lighting: Light Emitting Diodes vs. High Intensity Discharge Fixtures," *PLOS ONE*, vol. 9, no. 6, p. e99010, Jun. 2014. https://doi.org/10.1371/journal.pone.0099010.
[4] J. A. Teixeira da Silva, M. M. Hossain, M. Sharma, J. Dobránszki, J. C. Cardoso, and S. Zeng, "Acclimatization of *in Vitro*-derived *Dendrobium*," *Horticultural Plant Journal*, vol. 3, no. 3, pp. 110–124, May 2017. https://doi.org/10.1016/j.hpj.2017.07.009
[5] S. Chandra, R. Bandopadhyay, V. Kumar, and R. Chandra, "Acclimatization of tissue cultured plantlets: from laboratory to land," *Biotechnol Lett*, vol. 32, no. 9, pp. 1199–1205, Sep. 2010. https://doi.org/10.1007/s10529-010-0290-0
[6] M. A. Akkaş and R. Sokullu, "An IoT-based greenhouse monitoring system with Micaz motes," *Procedia Computer Science*, vol. 113, pp. 603–608, Jan. 2017. https://doi.org/10.1016/j.procs.2017.08.300
[7] A. F. Subahi and K. E. Bouazza, "An Intelligent IoT-Based System Design for Controlling and Monitoring Greenhouse Temperature," *IEEE Access*, vol. 8, pp. 125488–125500, 2020. https://doi.org/10.1109/ACCESS.2020.3007955
[8] C. Bersani, C. Ruggiero, R. Sacile, A. Soussi, and E. Zero, "Internet of Things Approaches for Monitoring and Control of Smart Greenhouses in Industry 4.0," *Energies*, vol. 15, no. 10, p. 3834, Jan. 2022. https://doi.org/10.3390/en15103834
[9] A. Guney and O. Cakir, "Design and Temperature Control of a Novel Aeroponic Plant Growth Chamber," *Electronics*, vol. 14, no. 14, p. 2801, Jan. 2025. https://doi.org/10.3390/electronics14142801
[10] N. Singh, A. K. Sharma, I. Sarkar, S. Prabhu, and K. Chadaga, "IoT-based greenhouse technologies for enhanced crop production: a comprehensive study of monitoring, control, and communication techniques," *Systems Science & Control Engineering*, vol. 12, no. 1, p. 2306825, Dec. 2024. https://doi.org/10.1080/21642583.2024.2306825
[11] H. Li, Y. Guo, H. Zhao, Y. Wang, and D. Chow, "Towards automated greenhouse: A state of the art review on greenhouse monitoring methods and technologies based on internet of things," *Computers and Electronics in Agriculture*, vol. 191, p. 106558, Dec. 2021. https://doi.org/10.1016/j.compag.2021.106558
[12] M. Cicioğlu and A. Çalhan, "Smart agriculture with internet of things in cornfields," *Computers & Electrical Engineering*, vol. 90, p. 106982, Mar. 2021. https://doi.org/10.1016/j.compeleceng.2021.106982
[13] H. Benyezza, M. Bouhedda, R. Kara, and S. Rebouh, "Smart platform based on IoT and WSN for monitoring and control of a greenhouse in the context of precision agriculture," *Internet of Things*, vol. 23, p. 100830, Oct. 2023. https://doi.org/10.1016/j.iot.2023.100830
[14] Y. R. Suradinata, Murgayanti, E. Suminar, A. Nuraini, J. S. Hamdani, and S. Mubarok, "Data on the vegetative growth at post acclimatization stage of two *dendrobium* genotypes as an effect of different growing media," *Data in Brief*, vol. 26, p. 104493, Oct. 2019. https://doi.org/10.1016/j.dib.2019.104493
[15] M. Goldfarb and T. Sirithanapipat, "The effect of actuator saturation on the performance of PD-controlled servo systems," *Mechatronics*, vol. 9, no. 5, pp. 497–511, Aug. 199. https://doi.org/10.1016/S0957-4158(99)00013-6
[16] S. Adla, N. K. Rai, S. H. Karumanchi, S. Tripathi, M. Disse, and S. Pande, "Laboratory Calibration and Performance Evaluation of Low-Cost Capacitive and Very Low-Cost Resistive Soil Moisture Sensors," *Sensors*, vol. 20, no. 2, p. 363, Jan. 2020. https://doi.org/10.3390/s20020363